

# V<sub>2</sub>O<sub>5</sub> Nanowire Composite Paper as a High-Performance Lithium-Ion Battery Cathode

Yue Zhang,<sup>†,‡</sup> Yizhi Wang,<sup>‡</sup> Zhihong Xiong,<sup>†</sup> Yongming Hu,<sup>\*,†,§,¶</sup> Weixing Song,<sup>‡</sup> Qiu-an Huang,<sup>†</sup> Xiaoxing Cheng,<sup>§</sup> Long-Qing Chen,<sup>§</sup> Chunwen Sun,<sup>‡,¶</sup> and Haoshuang Gu<sup>\*,†</sup>

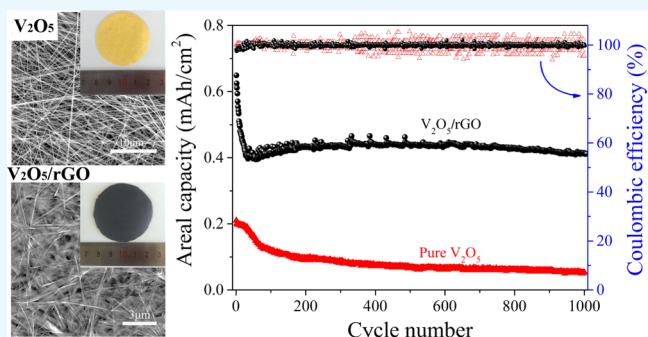
<sup>†</sup>Hubei Collaborative Innovation Center for Advanced Organic Chemical Materials; Hubei Key Laboratory of Ferro & Piezoelectric Materials and Devices; Faculty of Physics & Electronic Science, Hubei University, Wuhan 430062, P. R. China

<sup>‡</sup>Beijing Institute of Nanoenergy and Nanosystems, Chinese Academy of Sciences, National Center for Nanoscience and Technology (NCNST), Beijing 100083, P. R. China

<sup>§</sup>Department of Materials Science & Engineering, The Pennsylvania State University, University Park, Pennsylvania 16802, United States

## S Supporting Information

**ABSTRACT:** Ultralong, as long as ~1 mm, orthorhombic vanadium pentoxide (V<sub>2</sub>O<sub>5</sub>) nanowires were synthesized using a hydrothermal method. Free-standing and binder-free composite paper was prepared on a large scale by a two-step reduction method using free-standing V<sub>2</sub>O<sub>5</sub> nanowires as the skeleton and reduced graphene oxide (rGO) nanosheets as the additive. Such a free-standing V<sub>2</sub>O<sub>5</sub>/rGO composite paper as a cathode for lithium ion batteries possesses both structural integrity and extraordinary electrochemical performance. The reversible specific areal capacity of the V<sub>2</sub>O<sub>5</sub>/rGO composite paper electrode is 885 μAh/cm<sup>2</sup> at 0.09 mA/cm<sup>2</sup>, much higher than that of the pure V<sub>2</sub>O<sub>5</sub> nanowire paper electrode (570 μAh/cm<sup>2</sup>). It also shows excellent cycling performance at high rates with 30.9% loss of its initial capacities after 1000 cycles at a current rate of 0.9 mA/cm<sup>2</sup>. The excellent performance was attributed to the improved electronic conductivity and Li<sup>+</sup> ion transport from the rGO addition.



## INTRODUCTION

Currently, lithium ion batteries (LIBs) have been considered as the leading candidates for new energy vehicles, hybrid cars, and various portable and smart devices because of their high-energy density and long lifetime. So far, different metal oxides have been explored as cathode materials, such as LiCoO<sub>2</sub>, LiFePO<sub>4</sub>, TiO<sub>2</sub>, etc.<sup>1–3</sup> However, those electrode materials based on conventional transitional metal oxides still suffer from poor performance; it is a huge challenge to improve the specific capacities/energy densities to meet the increasing demands of electronic devices and electronic vehicles. Moreover, the electrode materials in conventional LIBs are typically in a powder form, and thus they require conductive additives, insulated polymer binders, and aluminum or copper foil current collectors. Those inactive ingredients significantly decreased the overall energy and power density of the electrodes, besides increasing the costs.<sup>4</sup> To improve the performance of LIBs, designing a new kind of free-standing and binder-free electrodes in which all of the materials contribute to the lithium storage is an effective strategy. Meanwhile, great efforts have been devoted to designing original electrodes and decreasing the inactive additives in the electrodes.<sup>5–7</sup>

Among the explored LIB cathode materials, vanadium pentoxide (V<sub>2</sub>O<sub>5</sub>) is a promising candidate due to its high capacity, stable crystal structure, and low cost. However, its low electronic conductivity, small diffusion coefficient of Li ions, poor rate capability, and cycle stability hinder the practical application of V<sub>2</sub>O<sub>5</sub> in LIBs.<sup>8</sup> In addition, the lithiation/delithiation processes in crystalline V<sub>2</sub>O<sub>5</sub> are also accompanied by structural phase transitions, which induce lattice strain within the same electrodes.<sup>9</sup> Nanostructuring of V<sub>2</sub>O<sub>5</sub>,<sup>10,11</sup> or modified V<sub>2</sub>O<sub>5</sub>,<sup>12,13</sup> adding carbon nanotubes,<sup>7,14</sup> graphene sheets, and reduced graphene oxide (rGO) nanosheets,<sup>6,15–18</sup> has been reported to improve the electrochemical behavior of V<sub>2</sub>O<sub>5</sub>. Furthermore, most of the studied materials for particularly positive electrodes as free-standing and binder-free electrodes are currently based on the rGO paper,<sup>6,18–21</sup> in which the amount of active material is very limited. It is well known that rGO in the composite material is helpful in improving the electronic conductivity of the active material, that is, those rGO-based paper electrodes do not possess good

Received: January 11, 2017

Accepted: February 22, 2017

Published: March 6, 2017

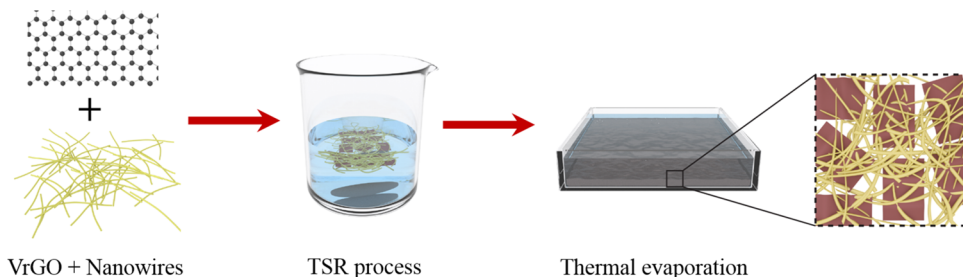


**Figure 1.** Schematic diagram showing the formation process of the  $\text{V}_2\text{O}_5/\text{rGO}$  composite paper.

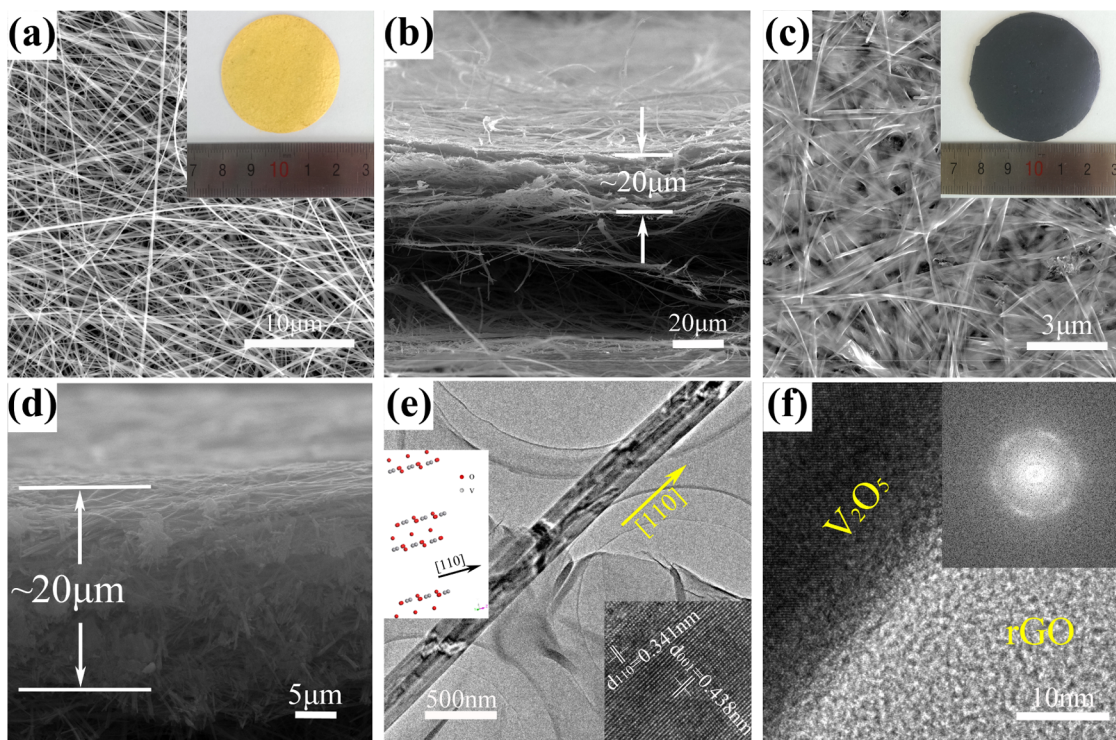


**Figure 2.** Top view and cross-sectional SEM images of (a, b) the surface and cross-section SEM images of the pure  $\text{V}_2\text{O}_5$  NWs paper and (c, d) the surface and cross-section SEM images of the  $\text{V}_2\text{O}_5/\text{rGO}$  composite paper (inset: digital picture). (e) TEM image of the  $\text{V}_2\text{O}_5/\text{rGO}$  composite paper (inset: HRTEM image of  $\text{V}_2\text{O}_5$  nanowire) and (f) HRTEM image of  $\text{V}_2\text{O}_5/\text{rGO}$  (inset: FFT diffraction of rGO).

energy density. Therefore, in this work, a free-standing composite paper with a diameter of several centimeters was successfully prepared on a large scale by a two-step reduction (TSR) method using ultralong  $\text{V}_2\text{O}_5$  nanowires serving as the skeleton and rGO nanosheets as the electronic transport network, as shown in the schematic diagram in Figure 1. The ultralong  $\text{V}_2\text{O}_5$  nanowires were retained, and a layer-by-layer structured composite is obtained finally. More importantly, this process is simple, reproducible, and can be scaled-up, which is very important for practical applications. As a cathode for LIBs, the free-standing  $\text{V}_2\text{O}_5$  nanowire composite paper electrodes show excellent electrochemical performances.

## RESULTS AND DISCUSSION

The  $\text{V}_2\text{O}_5$  nanowire paper and the  $\text{V}_2\text{O}_5/\text{rGO}$  composite paper were prepared using the TSR method; the corresponding scanning electron microscopy (SEM) images are shown in Figure 2a–d. As can be seen, both of them are composed of free-standing nanowires, and the formed flexible papers have a diameter of 4.0 cm and a thickness of about 20  $\mu\text{m}$ . It is obvious that the ultralong  $\text{V}_2\text{O}_5$  nanowires distributed

randomly within the pure paper and interconnected with each other to form a network; the length of an individual nanowire reaches up to 1.0 mm, as shown in Figure 2a,b. It can also be observed that a large amount of  $\text{V}_2\text{O}_5$  nanowires interweave and interact with rGO sheets to form a dense structure (Figure 2c,d). The cross-sectional view further reveals that the  $\text{V}_2\text{O}_5$  nanowires and rGO sheets interlace with each other to form a multilayered stacking structure. In addition, the as-prepared  $\text{V}_2\text{O}_5/\text{rGO}$  composite paper exhibits a rough and porous surface, and the tight fit between the  $\text{V}_2\text{O}_5$  nanowires and the rGO sheets may be beneficial for the cycling performance.<sup>6</sup> For comparison, Figure S2 shows the SEM images of the  $\text{V}_2\text{O}_5$  nanowires combined with Super P ( $\text{V}_2\text{O}_5/\text{SP}$ ); one can see that the composite is quite inhomogeneous. Figure 2e shows the transmission electron microscopy (TEM) image of the  $\text{V}_2\text{O}_5/\text{rGO}$  composite paper in a few layers. The rGO nanosheets with their characteristic wrinkles can be distinguished easily and clearly demonstrate that the  $\text{V}_2\text{O}_5$  nanowires serve as the skeleton, and the rGO nanosheets serve as the additive. The inset is a high-resolution transmission electron microscopy (HRTEM) image of an individual  $\text{V}_2\text{O}_5$

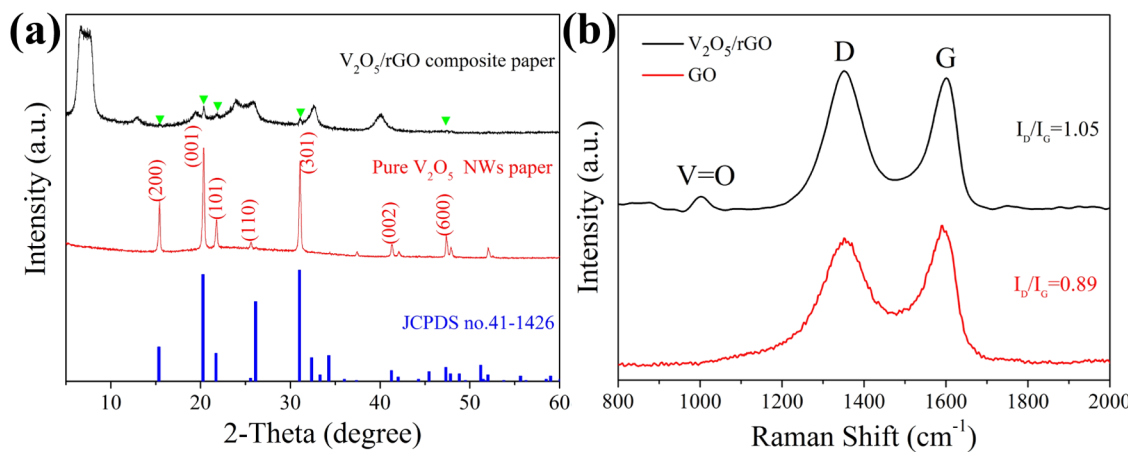


**Figure 3.** (a) XRD patterns of the pure V<sub>2</sub>O<sub>5</sub> nanowire paper and the V<sub>2</sub>O<sub>5</sub>/rGO composite paper and (b) the Raman spectrum of the V<sub>2</sub>O<sub>5</sub>/rGO composite paper and GO nanosheets.

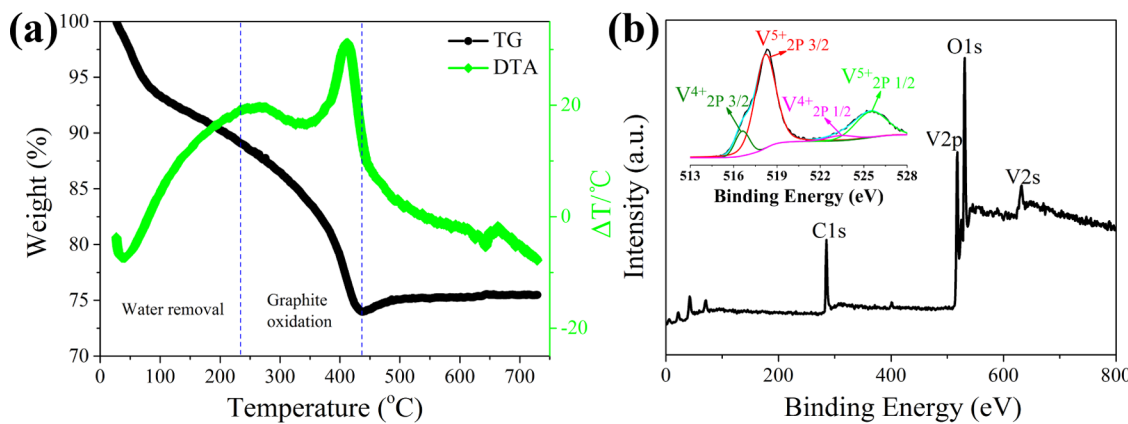


**Figure 4.** (a) TGA curve and (b) XPS survey spectrum of the V<sub>2</sub>O<sub>5</sub>/rGO composite paper.

nanowire, with a characteristic lattice spacing of 0.341 and 0.438 nm, corresponding to the (110) and (001) planes of the orthorhombic-phase V<sub>2</sub>O<sub>5</sub>, respectively.<sup>7</sup> It is noted that the V<sub>2</sub>O<sub>5</sub> nanowires are grown along the [110] direction. Figure 2f presents the HRTEM image of the V<sub>2</sub>O<sub>5</sub>/rGO composite and the fast Fourier transform (FFT) pattern of rGO, the almost regular hexagonal diffraction pattern indicating the good carbon framework of rGO.<sup>23</sup>

The X-ray diffraction (XRD) patterns of the V<sub>2</sub>O<sub>5</sub> nanowire paper and the V<sub>2</sub>O<sub>5</sub>/rGO composite paper are shown in Figure 3a. The pure V<sub>2</sub>O<sub>5</sub> nanowire paper features diffraction peaks of (200), (001), (101), (110), (301), (002), and (600) corresponding to the orthorhombic-phase V<sub>2</sub>O<sub>5</sub> (JCPDS No. 41-1426).<sup>18</sup> However, for V<sub>2</sub>O<sub>5</sub>/rGO composites, three additional wide diffraction peaks located at around 7, 33, and 40° were observed besides the V<sub>2</sub>O<sub>5</sub> phase, which can be attributed to the dehydrated phase of V<sub>2</sub>O<sub>5</sub> (JCPDS No. 40-1296) produced in the liquid-phase synthesis.<sup>28–30</sup> Meanwhile, the characteristic diffraction peak located at 26° belongs to the phase of rGO.<sup>28</sup> In order to remove the physically absorbed water within the composite, the samples were annealed at 210 °C and keep the physical property of rGO simultaneously. One can see that the physically absorbed water disappeared after heat treatment, whereas the hydration water remained within V<sub>2</sub>O<sub>5</sub>, which can transfer into pure orthorhombic-phase V<sub>2</sub>O<sub>5</sub> completely after annealing at 450 °C for 6 h in air, while the rGO in the composite would be burned (as shown in Figure

S3). Figure 3b shows the Raman spectra of the V<sub>2</sub>O<sub>5</sub>/rGO nanowire composite paper and the GO nanosheets, which provide further evidence for the coexistence of rGO sheets and V<sub>2</sub>O<sub>5</sub> nanowires. As can be seen, two predominant peaks appear at about 1347 and 1596 cm<sup>-1</sup> in the spectrum, assigned as the D band originating from the disordered carbon and the G band corresponding to the sp<sup>2</sup> hybridized carbon, respectively. A slightly higher D/G ratio ( $I_D/I_G = 1.06$ ) was obtained for the V<sub>2</sub>O<sub>5</sub>/rGO composite compared to that of the GO nanosheets ( $I_D/I_G = 0.89$ ), indicating that the TSR process removed the oxygen-containing functional groups effectively and reformed the structure of GO with a good quantity.<sup>19</sup> The peaks centered at 995 cm<sup>-1</sup> related to the V=O stretching vibration of V<sub>2</sub>O<sub>5</sub>,<sup>7,19</sup> indicating the presence of V<sub>2</sub>O<sub>5</sub> in the composite paper. In addition, the Raman spectrum of the pure V<sub>2</sub>O<sub>5</sub> nanowires is shown in Figure S4; the spectrum fits well with the reported literature.<sup>7,10</sup>

To determine the percentage of graphene content within the V<sub>2</sub>O<sub>5</sub>/rGO composite, a thermal gravimetric analysis (TGA) curve was obtained. As shown in Figure 4a, the first weight loss is about 11% at around 230 °C, which may be ascribed to the physisorbed and chemisorbed water on the surface of the V<sub>2</sub>O<sub>5</sub>/rGO composite paper. The second weight loss is ~13% from 230 to 440 °C, which most likely corresponds to the oxidation of graphene. It should be mentioned that a slight increase in weight is observed in the curve at around 450 °C; this may relate to the transformation of a few VO<sub>2</sub> molecules

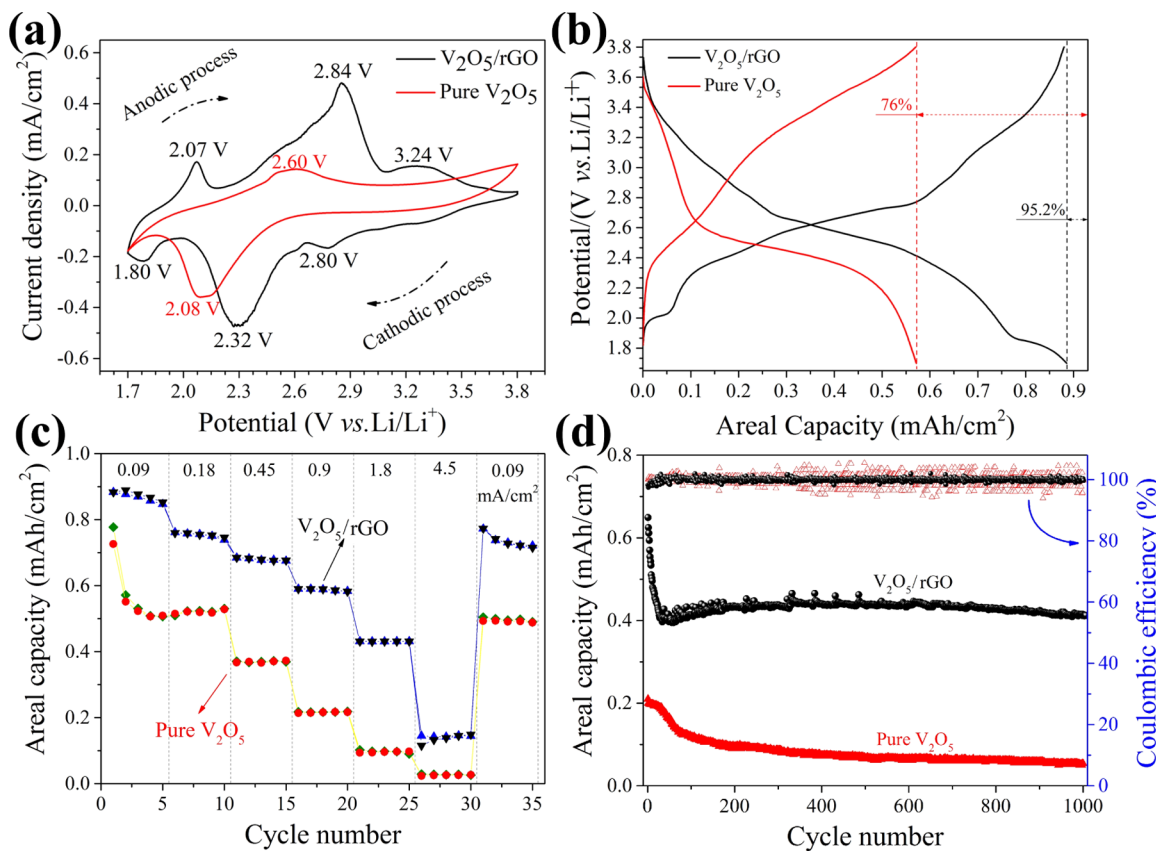


**Figure 5.** (a) Representative CV curves of the pure V<sub>2</sub>O<sub>5</sub> nanowire paper and the V<sub>2</sub>O<sub>5</sub>/rGO composite paper electrodes obtained at a voltage range of 1.7–3.8 V (vs Li<sup>+</sup>/Li) and a potential scan rate of 0.1 mV/s. (b) Voltage profiles for the pure V<sub>2</sub>O<sub>5</sub> nanowire paper and the V<sub>2</sub>O<sub>5</sub>/rGO composite paper electrodes at a current rate of 0.09 mA/cm<sup>2</sup>. (c) Discharge/charge capability of the pure V<sub>2</sub>O<sub>5</sub> nanowire paper and the V<sub>2</sub>O<sub>5</sub>/rGO composite paper electrodes at various rates for 35 cycles. (d) Capacity (left) and efficiency (right) vs cycle number for the pure V<sub>2</sub>O<sub>5</sub> nanowire paper and the V<sub>2</sub>O<sub>5</sub>/rGO composite paper electrodes at a current rate of 0.9 mA/cm<sup>2</sup>.

into V<sub>2</sub>O<sub>5</sub>. Excluding the weight loss of water molecule, the weight contents of V<sub>2</sub>O<sub>5</sub> were about 85 wt % in the V<sub>2</sub>O<sub>5</sub>/rGO composites, in good agreement with the synthetic experiment.<sup>7,28,31</sup> The higher proportion of V<sub>2</sub>O<sub>5</sub> in the free-standing electrodes will result in higher energy density (as shown in the Supporting information, Tables S1 and S2). Figure 4b shows the survey X-ray photoelectron spectroscopy (XPS) spectrum of the composites in the binding energy range of 0–800 eV. It can be seen that the composite contains V, O, and C elements, corresponding to the binding energy of 517.5, 530.4, and 285 eV, respectively; no other elements are detected. The binding energy of vanadium and oxygen as determined by the XPS spectra indicated the formation of V-oxides in the composites.<sup>7,20</sup> The C 1s XPS spectrum of the V<sub>2</sub>O<sub>5</sub>/rGO composite paper sample, shown in Figure S5, indicates that good quality of rGO is synthesized from the TSR method.

To evaluate the electrochemical behavior of the paper electrodes for LIB applications, the pure V<sub>2</sub>O<sub>5</sub> nanowire paper and the V<sub>2</sub>O<sub>5</sub>/rGO composite paper were cut into small pellets ( $\varnothing$  9 mm) and used as cathodes in coin-type cells directly. Figure 5a shows typical cyclic voltammetry (CV) curves obtained at room temperature (RT) between 1.7 and 3.8 V (vs Li/Li<sup>+</sup>) at a scan rate of 0.1 mV/s (this voltage range was chosen rather than the more conservative range of 2.0–4.0 V because it permits increased lithiation, which would bring the capacity close to the theoretical value).<sup>21,28,31</sup> Three pairs of well-defined redox peaks at 2.07, 2.84, and 3.24 V (vs Li/Li<sup>+</sup>) in the anodic process and 2.80, 2.32, and 1.80 V (vs Li/Li<sup>+</sup>) in the

cathodic process are observed from the CV curves. This can be assigned to the different stages during the Li<sup>+</sup> insertion process occurring at the V<sub>2</sub>O<sub>5</sub>/rGO composite paper electrodes, which could be expressed by the following equation: V<sub>2</sub>O<sub>5</sub> + xLi<sup>+</sup> + xe<sup>-</sup>  $\leftrightarrow$  Li<sub>x</sub>V<sub>2</sub>O<sub>5</sub>. More specifically, the first reduction peak at 3.24 V is attributed to the conversion of  $\alpha$ -V<sub>2</sub>O<sub>5</sub> into  $\epsilon$ -Li<sub>0.5</sub>V<sub>2</sub>O<sub>5</sub>;<sup>10,11,10,11</sup> subsequent reductions take place at 2.84 and 2.07 V, corresponding to the formation of  $\delta$ -Li<sub>2</sub>V<sub>2</sub>O<sub>5</sub> and  $\gamma$ -LiV<sub>2</sub>O<sub>5</sub>, respectively.<sup>28,32</sup> For comparison, the pure V<sub>2</sub>O<sub>5</sub> paper has only a couple of redox peaks, at 2.60 and 2.08 V (vs Li/Li<sup>+</sup>), due to its relatively poor conductivity.

Figure 5b shows the voltage profiles of the pure V<sub>2</sub>O<sub>5</sub> nanowire paper and the V<sub>2</sub>O<sub>5</sub>/rGO composite paper electrodes at a current rate of 0.09 mA/cm<sup>2</sup>, respectively. In agreement with the above CV results, the processes display multiple redox plateaus between 1.7 and 3.8 V, indicating the structural transformation from the  $\alpha$ -V<sub>2</sub>O<sub>5</sub> to  $\epsilon$ -Li<sub>0.5</sub>V<sub>2</sub>O<sub>5</sub> and  $\delta$ -Li<sub>2</sub>V<sub>2</sub>O<sub>5</sub> and finally to the  $\gamma$ -LiV<sub>2</sub>O<sub>5</sub> phase. It should be mentioned that the discharge- and charge-specific capacity are 0.885 and 0.880 mAh/cm<sup>2</sup>, which is up to 95.2% of the theoretical capacity of V<sub>2</sub>O<sub>5</sub> for two lithium intercalations (Figure S6).<sup>7</sup> However, the pure V<sub>2</sub>O<sub>5</sub> paper with lower electronic conductivity has a lower capacity of 0.570 mAh/cm<sup>2</sup>, which is still higher than that reported previously.<sup>3,33</sup> The electrical conductivity of the composite paper is about 1.62 S cm<sup>-1</sup>, which is 33 times higher than that of the pure V<sub>2</sub>O<sub>5</sub> nanowire paper (0.049 S cm<sup>-1</sup>). Therefore, the excellent performance could be attributed to the binder-free, the excellent electronic con-

ductivity of rGO, and the interconnected network of  $\text{V}_2\text{O}_5$  nanowires with good mechanical integrity, indicating that the free-standing electrode is very favorable for LIB applications.

To investigate their rate performances, various current densities ( $0.09\text{--}4.5 \text{ mA/cm}^2$ ) were applied on those paper electrodes as shown in Figure 5c. It is obvious that the areal capacity of the pure  $\text{V}_2\text{O}_5$  nanowire paper electrodes drops significantly with an increase in the discharge/charge rates. It should be noted that during the first cycle of discharge/charge, the pure  $\text{V}_2\text{O}_5$  nanowire paper electrodes present quite high areal capacity due to the unavoidable solid–electrolyte interphase (SEI) film formation on the electrode surface and some possible side reactions between  $\text{Li}^+$  and the residual functional groups in the rGO structure.<sup>34</sup> For comparison, the  $\text{V}_2\text{O}_5/\text{rGO}$  composite paper electrodes show a higher areal capacity and better rate capability than those of the pure  $\text{V}_2\text{O}_5$  nanowire paper electrodes. As the current densities are 0.18, 0.45, 0.9, and  $1.8 \text{ mA/cm}^2$ , the  $\text{V}_2\text{O}_5/\text{rGO}$  composite paper electrodes can deliver discharge capacities of 0.76, 0.68, 0.59, and  $0.43 \text{ mAh/cm}^2$ , respectively. It should be noted that a stable discharge capacity of  $0.742 \text{ mAh/cm}^2$  can be recovered as the current density returns to  $0.09 \text{ mA/cm}^2$ , suggesting the good structure stability of the sample after a high rate of discharge and charge.<sup>18</sup>

Figure 5d exhibits the cycling performance of the pure  $\text{V}_2\text{O}_5$  paper electrodes and the  $\text{V}_2\text{O}_5/\text{rGO}$  composite paper electrodes at a current density of  $0.9 \text{ mA/cm}^2$ . It is noted that the initial Coulombic efficiency (CE) of the first discharge and charge cycles is about 97%, which may also be attributed to the same unavoidable SEI film formation and the possible side reactions.<sup>34</sup> More importantly, the CE value reaches up to 99% after 30 cycles and maintains a stable value after 1000 cycles. A discharge capacity of  $0.415 \text{ mAh/cm}^2$  can be delivered after 1000 cycles at  $0.9 \text{ mA/cm}^2$ , corresponding to 69.1% of the initial discharge capacity. Without the binder, the  $\text{V}_2\text{O}_5$  nanowire network and the rGO bind together tightly (without structural damage) so that the rGO can keep the structure of  $\text{V}_2\text{O}_5$  from deterioration during the cycling process.<sup>35</sup> Lee et al. also mentioned that a voltage range of  $1.7\text{--}3.8 \text{ V}$  is suitable for the  $\text{V}_2\text{O}_5/\text{rGO}$  composite.<sup>21</sup> In contrast, the pure  $\text{V}_2\text{O}_5$  paper electrodes only retain about 28% of the initial discharge capacity at the current density of  $0.9 \text{ mA/cm}^2$  after 1000 cycles, which could be related to their poor rate capability and structural stability. For another comparison, the cycling performance of the  $\text{V}_2\text{O}_5/\text{SP}$  composite paper is quite poor after 1000 cycles (Figure S7). In addition, the  $\text{V}_2\text{O}_5/\text{rGO}$  composite paper still maintains good cycle stability at the current density of  $1.8 \text{ mA/cm}^2$ , that is, 55% after 1000 cycles (Figure S8), which reveals that the  $\text{V}_2\text{O}_5/\text{rGO}$  composite paper has excellent cycling performance.

Figure 6 shows the electrochemical impedance spectra (Nyquist plots) of both cells with the pure  $\text{V}_2\text{O}_5$  nanowire paper and the  $\text{V}_2\text{O}_5/\text{rGO}$  composite paper electrodes. The stable SEI layers were formed after several cycling processes for the pure  $\text{V}_2\text{O}_5$  nanowire paper cell and the  $\text{V}_2\text{O}_5/\text{rGO}$  composite paper cell, and two depressed semicircles and one slope tail were observed. The results were fitted well using the equivalent circuit shown in the inset in Figure 6.<sup>36</sup> The equivalent circuit consists of two parallel R-CPE circuits in series, one for the passive film formation and the other for lithium intercalation. Here,  $R_s$  is the Ohmic resistance related to the electrode, electrolyte, separator, and connection;  $R_1$  is often attributed to the impedance related to the SEI layer;  $R_2$  is the

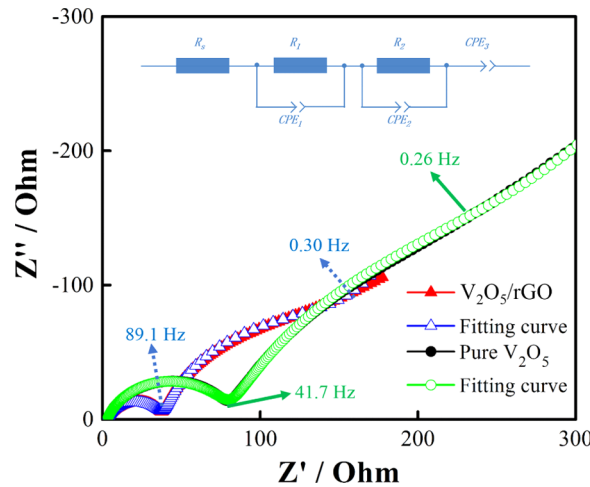


**Figure 6.** EIS (Nyquist plot) of the pure  $\text{V}_2\text{O}_5$  nanowire paper and the  $\text{V}_2\text{O}_5/\text{rGO}$  composite paper cells. Amplitude: 5 mV, frequency range: 10 mHz to 300 kHz.

charge-transfer reaction resistance, associated with Li intercalation and varies depending on the composition of the electrode.  $\text{CPE}_1$  and  $\text{CPE}_2$  represents the nonideal interfaces of the SEI layer and electrolyte–electrode, respectively.  $\text{CPE}_3$  is basically the Warburg impedance.<sup>37</sup>

$$Z_{\text{CPE}i} = \frac{1}{Q_i(j\omega)^{\alpha_i}}, \quad (i = 1, 2, 3)$$

where  $Q_i$  is the prefactor of the  $\text{CPE}i$ , and  $\alpha_i$  is its exponent. For the electrochemical impedance spectroscopy (EIS) measurement, the same procedures were followed for both cells under the same conditions, including the state of charge, the disturbing signal's amplitude, the frequency range, and the temperature. Table 1 shows the fitting parameters of the pure

**Table 1.** EIS Fitting Parameters of the Pure  $\text{V}_2\text{O}_5$  Nanowire Paper and the  $\text{V}_2\text{O}_5/\text{rGO}$  Composite Paper Electrodes

materials	$R_s$ ( $\Omega$ )	$R_1$ ( $\Omega$ )	$R_2$ ( $\Omega$ )
pure $\text{V}_2\text{O}_5$	3.0	76.8	165.3
$\text{V}_2\text{O}_5/\text{rGO}$	2.6	35.9	112

$\text{V}_2\text{O}_5$  nanowire paper and the  $\text{V}_2\text{O}_5/\text{rGO}$  composite paper electrodes according to the EIS measurement. It can be seen that the Ohmic resistance is reduced from 3.0 to  $2.6 \Omega$ , indicating that the conductivity of the electrodes is improved as rGO is introduced. The impedance related to the SEI layer ( $R_1$ ) is reduced from 76.8 to  $35.9 \Omega$  (reduced by almost half), indicating that rGO significantly improved the ion conductivity of the SEI layer. The charge-transfer reaction resistance ( $R_2$ ) is reduced from 165.3 to  $112 \Omega$ , demonstrating that the conductivity is improved after rGO is introduced. Thus, the AC impedance results further proved that the electrochemical performance of the  $\text{V}_2\text{O}_5/\text{rGO}$  composite paper is better than that of the pure  $\text{V}_2\text{O}_5$  nanowire paper electrodes.

## CONCLUSIONS

In summary, ultralong  $\text{V}_2\text{O}_5$  nanowires were synthesized by a hydrothermal process, and free-standing and binder-free pure  $\text{V}_2\text{O}_5$  nanowire paper and  $\text{V}_2\text{O}_5/\text{rGO}$  composite paper were prepared by the TSR method and were cut into small pellets used as a cathode for LIBs. The  $\text{V}_2\text{O}_5/\text{rGO}$  composite paper

electrode shows a higher specific capacity of 0.885 mAh/cm<sup>2</sup> at 0.09 mA/cm<sup>2</sup>, which can deliver discharge capacities of approximately 0.76, 0.68, 0.59, and 0.43 mAh/cm<sup>2</sup> at current densities of 0.18, 0.45, 0.9, and 1.8 mA/cm<sup>2</sup>, respectively, and a stable discharge capacity of 0.742 mAh/cm<sup>2</sup> can be recovered when the current density comes back to 0.09 mA/cm<sup>2</sup>. A 30.9% decay was observed in the capacity after 1000 cycles at 0.9 mA/cm<sup>2</sup> for the V<sub>2</sub>O<sub>5</sub>/rGO composite paper electrode. The results demonstrate that the free-standing V<sub>2</sub>O<sub>5</sub>/rGO composite paper is a promising cathode material for high-energy-density lithium batteries.

## METHODS

**Preparation of Ultralong V<sub>2</sub>O<sub>5</sub> Nanowires and Partial rGO Sheets.** Into a vessel of 50 mL Teflon (polytetrafluoroethylene) (PTFE)) with 35 mL of deionized (DI) water, 0.002 mol (0.364 g) of V<sub>2</sub>O<sub>5</sub> powders were added, then 5 mL of H<sub>2</sub>O<sub>2</sub> (30%) was dropped into the mixed solution slowly. After the solution was vigorously stirred for half an hour, the vessel was sealed into a homemade autoclave and placed in a stainless steel tank to perform a hydrothermal reaction at 230 °C for 12 h. After the autoclave was cooled down to RT naturally, the products were washed with DI water and ethanol several times and then dried at 100 °C in vacuum for 4 h. Finally, V<sub>2</sub>O<sub>5</sub> ultralong nanowires were obtained after the above products were calcined at 400 °C for 3 h in air.<sup>22</sup>

The graphene oxides were prepared by an improved synthesis process.<sup>23,24</sup> Following this, 21 mg of GO was dispersed in 21 mL of DI water, and then 21 mg of ascorbic acid was added into the dispersion; this mixture was subjected to ultrasonic treatment for 2 h. After allowing the dispersion to stand for 24 h, the mixture gradually turned black in color, and the ascorbic acid (Vitamin C)-reduced GO (VrGO) product was obtained.<sup>25,26</sup> This reduction of GO to VrGO is the first step.

**Preparation of the V<sub>2</sub>O<sub>5</sub>/rGO Composite Paper.** First, 119 mg of V<sub>2</sub>O<sub>5</sub> nanowires and 21 mL of as-synthesized VrGO (15 wt %) were dispersed in 119 mL of DI water completely under vigorous stirring for 1 h. Then, the mixture was transferred into the Teflon-lined autoclave, and another hydrothermal treatment was performed at 160 °C for 4 h. This in situ reduction of VrGO to rGO is the second step. The TSR process will tightly entangle the rGO and V<sub>2</sub>O<sub>5</sub> nanowires together.<sup>27</sup> Second, the product was washed with DI water and ethanol several times and transferred into a PTFE evaporating dish and heat-treated at 60 °C for 24 h. Finally, the V<sub>2</sub>O<sub>5</sub>/rGO composite paper was obtained by peeling it off from the PTFE evaporating dish. For comparison, another conductive additive, conductive carbon black (SP conductive 99+, abbr. SP, metal basis, Alfa Aesar China), was combined with the V<sub>2</sub>O<sub>5</sub> nanowire using a similar method without any other additive to synthesize the free-standing and binder-free V<sub>2</sub>O<sub>5</sub>/SP (15 wt %) composite paper. The pure V<sub>2</sub>O<sub>5</sub> nanowire paper was also prepared by a similar procedure as described above but in the absence of GO.

**Structural and Electrochemical Measurements.** The phase structures were characterized by XRD (AXS D8, Bruker) with Cu K $\alpha$  radiation ( $\lambda = 1.5406 \text{ \AA}$ ) over the  $2\theta$  range of 5–60°. The morphology and microstructure of the samples were examined by SEM (JSM-7100F) and TEM (FEI Tecnai G<sup>2</sup> F20). The weight percentages of rGO in the composite paper were determined by the thermogravimetric/differential thermal analyzer (TGA; Diamond TG/DTA, Perkin Elmer) with a

heating rate of 10 °C min<sup>-1</sup> from RT to 750 °C in air. The Raman spectrum (NTEGRA Spectra, NT-MDT) was used to study the phonon vibration behavior of the samples. The conductivity of the paper electrodes was tested by a four-point probe equipment (Tonghui TH2661). Without the binder and current collector, the free-standing pure V<sub>2</sub>O<sub>5</sub> nanowire paper, V<sub>2</sub>O<sub>5</sub>/SP, and V<sub>2</sub>O<sub>5</sub>/rGO composite paper were cut into small pellets ( $\phi = 9 \text{ mm}$ ), with an areal density of 2.5, 2.7, and 3.1 mg/cm<sup>2</sup>, respectively (Figure S1), and used as the cathode electrodes directly. Before fabrication of the lithium battery, the paper electrodes were annealed at 210 °C for 6 h. Coin-type cells (CR 2032) were assembled in an argon-filled glove box (MBraun), using the Li foil as the counter electrode and reference electrodes, 1 mol/L LiPF<sub>6</sub> in a mixture of ethylene carbonate and dimethyl carbonate (1:1 in volume) as the electrolyte, and glass microfiber filters (Whatman) as the separator. The electrochemical performances of the prepared electrodes were tested with a Land CT2001A tester system at RT. The cells were galvanostatically discharged and charged at different current densities in a voltage range of 1.7–3.8 V (vs Li<sup>+</sup>/Li). CV measurements were performed using the AutoLab (PGSTAT302N) electrochemical system at a scan rate of 0.1 mV/s, and the EIS of these cells were tested with a frequency range of 10 mHz to 300 kHz with an amplitude of 5 mV.

## ASSOCIATED CONTENT

### Supporting Information

The Supporting Information is available free of charge on the ACS Publications website at DOI: [10.1021/acsomega.7b00037](https://doi.org/10.1021/acsomega.7b00037).

Digital camera pictures; SEM characterization and XRD patterns of V<sub>2</sub>O<sub>5</sub>/SP composite paper; Raman spectrum; C 1s XPS spectrum; specific capacity of V<sub>2</sub>O<sub>5</sub>/rGO composite paper; electrochemical performance comparison of V<sub>2</sub>O<sub>5</sub>/rGO composite paper to the data published in the literatures (PDF)

## AUTHOR INFORMATION

### Corresponding Authors

\*E-mail: [huym@hubu.edu.cn](mailto:huym@hubu.edu.cn) (Y.H.).

\*E-mail: [guhsh@hubu.edu.cn](mailto:guhsh@hubu.edu.cn) (H.G.).

### ORCID

Yongming Hu: [0000-0002-0074-8305](https://orcid.org/0000-0002-0074-8305)

Chunwen Sun: [0000-0002-3610-9396](https://orcid.org/0000-0002-3610-9396)

### Notes

The authors declare no competing financial interest.

## ACKNOWLEDGMENTS

The authors acknowledge the financial support of the National Science Foundation of China (Nos. 61274073, 51172275, 11474088, and 51372271) and the National Key Basic Research Program of China (No. 2012CB215402). This work was also supported by the Thousands Talents Program for the pioneer researcher and his innovation team in China.

## REFERENCES

- (1) Yamada, A.; Chung, S. C.; Hinokuma, K. *J. Electrochem. Soc.* **2001**, *148*, A224–A229.
- (2) Ohzuku, T.; Ueda, A. *J. Electrochem. Soc.* **1994**, *141*, 2972–2977.
- (3) Mai, L.; Dong, F.; Xu, X.; Luo, Y.; An, Q.; Zhao, Y.; Pan, J.; Yang, J. *Nano Lett.* **2013**, *13*, 740–745.
- (4) Wang, S.; Xia, L.; Yu, L.; Zhang, L.; Wang, H.; Lou, X. W. *Adv. Energy Mater.* **2015**, *6*, No. 1502217.

- (5) Pushparaj, V. L.; Shaijumon, M. M.; Kumar, A.; Murugesan, S.; Ci, L.; Vajtai, R.; Linhardt, R. J.; Nalamasu, O.; Ajayan, P. M. *Proc. Natl. Acad. Sci. U.S.A.* **2007**, *104*, 13574–13577.
- (6) Wang, B.; Li, X.; Luo, B.; Jia, Y.; Zhi, L. *Nanoscale* **2013**, *5*, 1470–1474.
- (7) Kong, D.; Li, X.; Zhang, Y.; Hai, X.; Wang, B.; Qiu, X.; Song, Q.; Yang, Q.-H.; Zhi, L. *Energy Environ. Sci.* **2016**, *9*, 906–911.
- (8) Gittleson, F. S.; Hwang, J.; Sekol, R. C.; Taylor, A. D. *J. Mater. Chem. A* **2013**, *1*, 7979–7984.
- (9) Liu, Q.; Li, Z.-F.; Liu, Y.; Zhang, H.; Ren, Y.; Sun, C.-J.; Lu, W.; Zhou, Y.; Stanciu, L.; Stach, E. A.; Xie, J. *Nat. Commun.* **2015**, *6*, No. 6127.
- (10) Chen, M.; Xia, X.; Yuan, J.; Yin, J.; Chen, Q. *J. Power Sources* **2015**, *288*, 145–149.
- (11) Bai, H.; Liu, Z.; Sun, D. D.; Chan, S. H. *Energy* **2014**, *76*, 607–613.
- (12) Li, Y.; Yao, J.; Uchaker, E.; Zhang, M.; Tian, J.; Liu, X.; Cao, G. *J. Phys. Chem. C* **2013**, *117*, 23507–23514.
- (13) Yan, D.-J.; Zhu, X.-D.; Wang, K.-X.; Gao, X.-T.; Feng, Y.-J.; Sun, K.-N.; Liu, Y.-T. *J. Mater. Chem. A* **2016**, *4*, 4900–4907.
- (14) Chen, Z.; Augustyn, V.; Jia, X.; Xiao, Q.; Dunn, B.; Lu, Y. *ACS Nano* **2012**, *6*, 4319–4327.
- (15) Gao, X.-T.; Zhu, X.-D.; Le, S.-R.; Yan, D.-J.; Qu, C.-Y.; Feng, Y.-J.; Sun, K.-N.; Liu, Y.-T. *ChemElectroChem* **2016**, *3*, 1727–1959.
- (16) Liu, H.; Yang, W. *Energy Environ. Sci.* **2011**, *4*, 4000–4008.
- (17) Rui, X.; Zhu, J.; Sim, D.; Xu, C.; Zeng, Y.; Hng, H. H.; Lim, T. M.; Yan, Q. *Nanoscale* **2011**, *3*, 4752–4758.
- (18) Cheng, J.; Wang, B.; Xin, H. L.; Yang, G.; Cai, H.; Niea, F.; Huang, H. *J. Mater. Chem. A* **2013**, *1*, 10814–10820.
- (19) Perera, S. D.; Liyanage, A. D.; Nijem, N.; Ferraris, J. P.; Chabal, Y. J.; Balkus, K. J. *J. Power Sources* **2013**, *230*, 130–137.
- (20) Foo, C. Y.; Sumboja, A.; Tan, D. J. H.; Wang, J.; Lee, P. S. *Adv. Energy Mater.* **2014**, *4*, No. 1400236.
- (21) Lee, J. W.; Lim, S. Y.; Jeong, H. M.; Hwang, T. H.; Kang, J. K.; Choi, J. W. *Energy Environ. Sci.* **2012**, *5*, 9889–9894.
- (22) Zhai, T.; Liu, H.; Li, H.; Fang, X.; Liao, M.; Li, L.; Zhou, H.; Koide, Y.; Bando, Y.; Golberg, D. *Adv. Mater.* **2010**, *22*, 2547–2552.
- (23) Marcano, D. C.; Kosynkin, D. V.; Berlin, J. M.; Smitkii, A.; Sun, Z.; Slesarev, A.; Alemany, L. B.; Lu, W.; Tour, J. M. *ACS Nano* **2010**, *4*, 4806–4814.
- (24) Huang, X.; Qi, X.; Boeyab, F.; Zhang, H. *Chem. Soc. Rev.* **2012**, *41*, 666–686.
- (25) Zhang, J.; Yang, H.; Shen, G.; Cheng, P.; Zhang, J.; Guo, S. *Chem. Commun.* **2010**, *46*, 1112–1114.
- (26) Moon, I. K.; Lee, J.; Ruoff, R. S.; Lee, H. *Nat. Commun.* **2010**, *1*, 73.
- (27) Ding, J. N.; Liu, Y. B.; Yuan, N. Y.; Ding, G. Q.; Fan, Y.; Yu, C. T. *Diamond Relat. Mater.* **2012**, *21*, 11–15.
- (28) Du, G.; Seng, K. H.; Guo, Z.; Liu, J.; Li, W.; Jia, D.; Jia, C.; Liu, Z.; Liu, H. *RSC Adv.* **2011**, *1*, 690–697.
- (29) Wang, Y.; Shang, H.; Chou, T.; Cao, G. *J. Phys. Chem. B* **2005**, *109*, 11361–11366.
- (30) Petkov, V.; Trikalitis, P. N.; Bozin, E. S.; Billinge, S. J. L.; Vogt, T.; Kanatzidis, M. G. *J. Am. Chem. Soc.* **2002**, *124*, 10157–10162.
- (31) Ren, X.; Shi, C.; Zhang, P.; Jiang, Y.; Liu, J.; Zhang, Q. *Mater. Sci. Eng., B* **2012**, *177*, 929–934.
- (32) Yang, Y.; Li, L.; Fei, H.; Peng, Z.; Ruan, G.; Tour, J. M. *ACS Appl. Mater. Interfaces* **2014**, *6*, 9590–9594.
- (33) Sun, Y.; Yang, S.-B.; Lv, L.-P.; Lieberwirth, I.; Zhang, L.-C.; Ding, C.-X.; Chen, C.-H. *J. Power Sources* **2013**, *241*, 168–172.
- (34) Wang, J.-G.; Zhou, D.; Jin, R.; Liu, X.; Li, X.; Shen, C.; Xie, K.; Kang, F.; Li, B.; Wei, B. *ACS Nano* **2016**, *10*, 6227–6234.
- (35) Li, T.; Beidaghi, M.; Xiao, X.; Huang, L.; Hu, Z.; Sun, W.; Chen, X.; Gogotsi, Y.; Zhou, J. *Nano Energy* **2016**, *26*, 100–107.
- (36) Piao, T.; Park, S.-M.; Doh, C.-H.; Moon, S.-I. *J. Electrochem. Soc.* **1999**, *146*, 2794–2798.
- (37) Huang, Q. A.; Park, S. M. *J. Phys. Chem. C* **2012**, *116*, 16939–16950.